

# Passive Synthetic Aperture Imaging with Limited Noise Sources

**Josselin Garnier**

Laboratoire de Probabilités et Modèles Aléatoires & Laboratoire Jacques-Louis Lions, Université Paris Diderot, 75205 Paris Cedex 13, France

E-mail: [garnier@math.univ-paris-diderot.fr](mailto:garnier@math.univ-paris-diderot.fr)

**Abstract.** We consider a passive synthetic aperture imaging problem. A single moving receiver antenna records random signals generated by one or several distant noise sources and backscattered by one or several reflectors. The sources emit noise signals modeled by stationary random processes. The reflectors can be imaged by summing the autocorrelation functions of the received signals computed over successive time windows, corrected for Doppler factors and migrated by appropriate travel times. In particular the Doppler effect plays an important role and it can be used for resolution enhancement. When the noise source positions are not known, the reflector can be localized with an accuracy proportional to the reciprocal of the noise bandwidth, even when only a very small number of sources are available. When the noise source positions are known, the reflector can be localized with a cross range resolution proportional to the carrier wavelength and inversely proportional to the length of the receiver trajectory (i.e., the synthetic aperture), and with a range resolution proportional to the reciprocal of the bandwidth, even with only one noise source.

PACS numbers: 78A46, 35Q60

*Keywords:* Passive imaging, wave propagation, synthetic aperture radar, correlation.

## 1. Introduction

We consider a passive synthetic aperture radar imaging problem. This kind of problems is motivated on the one hand by the growth of illumination sources of opportunity, such as broadcasting stations, mobile phone or wifi base stations, and on the other hand by the availability of low-cost receivers, that can be stationary [15, 16, 9] or moving [2, 9, 17, 27]. Moreover the numerical processing in synthetic aperture radar is nowadays achievable and may even be accelerated by using GPU computing [5]. In this paper we consider the situation in which a single moving receiver antenna with very broadband capacities records the signal generated by one or several distant noise sources and backscattered by one or several reflectors (see Figure 1). A noise source is a point-like source that emits an unknown signal, modeled as a stationary random process, its position may be known or unknown and we will address both cases. When there is one opportunistic source emitting repeatedly the same pulse, it has been shown that correlation-based techniques could be used to image reflectors [23, 24, 26, 27]. When there are many noise sources and the illumination is diversified enough, that is to say, when the noise sources are dense enough and are distributed in an extended region, it was shown in [13] that the reflectors can be imaged by migrating the autocorrelation functions of the received signals over successive time windows. The imaging method proposed in [13] follows the principle of seismic interferometry, in which a passive receiver array is used to perform travel-time tomography and reflector imaging using only ambient noise illumination [3, 10, 20, 25, 11, 12, 14].

In [13] the analysis was carried out under the stop-go approximation, which means that the velocity of the receiver antenna is small enough so that the receiver antenna can be assumed to be stationary during each time window. Under the stop-go approximation, it is shown in [13] that the reflectors can be imaged only if the illumination is rich and diversified. However, it is known that the stop-go approximation does not hold when the velocity of the antenna is too large and/or when the relevant time intervals are too long. As discussed for instance in [22] in the context of active synthetic aperture radar, in which the antenna is both the source and the receiver, there are two main effects that have to be taken into account. First the antenna may have moved during the relevant time interval, which is the round trip from the antenna to the target in the context of active synthetic aperture radar. Second the Doppler effect induces a frequency shift in the measured signals. This frequency shift must be included in the definition of the matched filter imaging function.

In this paper, we revisit the passive synthetic aperture radar imaging problem by taking into account and exploiting two original and important features:

- the number of sources can be very limited in practice. Indeed the case of extended noise sources corresponds to the underwater acoustics problem, in which there is a sheet of point-like noise sources just below the sea surface [21, 18, 19]. In radar the typical situation is the use of one or several noise or opportunistic sources [9]. This means that we should be able to address the case with only one point-like noise source and

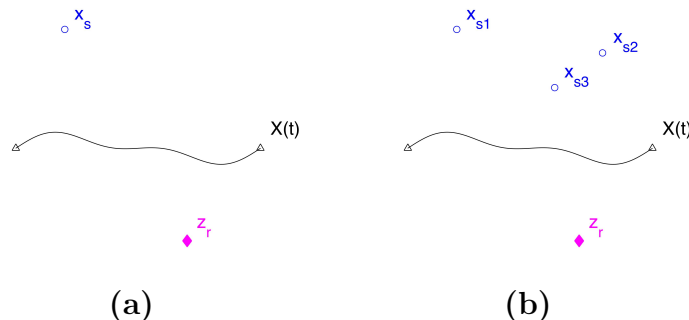


**Figure 1.** Passive sensor array imaging set up. In picture (a) the geometric set up with one source is plotted:  $\mathbf{x}_s$  is the source position,  $\mathbf{z}_r$  is the reflector position,  $(\mathbf{X}(t))_{t \in [0, T]}$  is the receiver antenna trajectory. In picture (b) the geometric set up with several (here three) sources is plotted.

then extend the result to multiple sources but in limited number, which is a situation complementary to the continuum approximation for the source distribution considered in [13].

- the Doppler effect cannot be neglected when the width of the time windows used to compute the autocorrelations becomes large. Indeed we will see that this time duration is the relevant one that determines the influence of the Doppler effect in the passive configuration, instead of the time for a round trip from the receiver antenna to the target in the active configuration. The choice of a small or large time window depends on the user. A priori the choice of a small time window could be thought to be appropriate as it could allow to avoid Doppler effects and to use the stop-go approximation as in [13]. However, the Doppler effect can in fact be useful in passive imaging, as already noticed in [23, 24, 26, 27], and it can be exploited by an appropriate imaging function in order to address the case of a limited number of sources. This is the main result of this paper.

The paper is organized as follows: In Section 2 we introduce the imaging function and summarize the main results. In Section 3 we carry out the high-frequency analysis of the imaging function and give its resolution properties when there is a single point-like noise source with unknown position. In Section 4 we extend the result to multiple unknown sources. Finally we introduce and study another imaging function that requires the knowledge of the source position in Section 5. Section 6 is devoted to numerical simulations that illustrate the main results of the paper.

## 2. Passive synthetic aperture imaging

### 2.1. Passive synthetic aperture imaging set up

In this paper we consider a two-dimensional situation. In this section we assume that there is a point-like noise source at  $\mathbf{x}_s$ , a single moving receiver antenna with the known trajectory  $(\mathbf{X}(t))_{t \in [0, T]}$ , and a point-like reflector at  $\mathbf{z}_r$  (see Figure 1(a)). The reflector

is modeled by a local change of the speed of propagation of the form

$$\frac{1}{c^2(\mathbf{x})} = \frac{1}{c_0^2}(1 + \sigma_r \mathbf{1}_{\Omega_r}(\mathbf{x} - \mathbf{z}_r)), \quad (1)$$

where  $\Omega_r$  is a small domain with volume  $l_r^2$  and  $\sigma_r$  is the reflectivity of the reflector.

The receiver antenna records

$$U_s(t) = u_s(t, \mathbf{X}(t)) \text{ for } t \in [0, T], \quad (2)$$

where  $u_s(t, \mathbf{x})$  is the wave field generated by the noise source at  $\mathbf{x}_s$ :

$$\frac{1}{c^2(\mathbf{x})} \frac{\partial^2 u_s}{\partial t^2} - \Delta_{\mathbf{x}} u_s = n_s(t) \delta(\mathbf{x} - \mathbf{x}_s), \quad (3)$$

with the speed of propagation of the form (1). The source term  $n_s(t)$  is the signal emitted by the noise source and we model it as a realization of a real-valued random process with mean zero and covariance of the form

$$\langle n_s(t) n_s(t') \rangle = F(t - t'). \quad (4)$$

Here  $\langle \cdot \rangle$  stands for statistical average with respect to the distribution of the noise source. For simplicity we consider that the process  $n_s$  has Gaussian statistics, whose distribution is characterized by the correlation function  $F(t - t')$ , which is a function of  $t - t'$  only, which means that the process is stationary. The Fourier transform  $\hat{F}(\omega)$  of the correlation function  $F(t)$  is a nonnegative, even, real-valued function proportional to the power spectral density of the noise sources:

$$\hat{F}(\omega) = \int_{\mathbb{R}} F(t) e^{i\omega t} dt. \quad (5)$$

The central frequency of the correlation function is denoted by  $\omega_0$  and its bandwidth is  $B$ . The correlation function has the form:

$$F(t) = F_B(t) e^{-i\omega_0 t} + cc, \quad \hat{F}(\omega) = \hat{F}_B(\omega - \omega_0) + \hat{F}_B(-\omega - \omega_0),$$

where  $F_B$  has bandwidth  $B$  and  $\hat{F}_B(\omega) \geq 0$  and  $cc$  stands for complex conjugate.

In a typical radar configuration with a flying platform,  $c_0 = 3 \cdot 10^8 \text{m.s}^{-1}$ ,  $\omega_0 \sim 2\pi \cdot 10^9 - 10^{10} \text{rad.s}^{-1}$ ,  $B \sim 2\pi \cdot 10^7 - 10^8 \text{rad.s}^{-1}$ , the typical propagation distance  $L$  is of the order of 10km. The velocity  $V$  of the receiver antenna is of the order of  $200 \text{m.s}^{-1}$  [6, 9].

In [13], the stop-go approximation was made. The receiver was supposed to be at the stationary position  $\mathbf{x}_j$  during the time interval  $[T_j, T_j + \Delta T]$  for the  $N$  successive positions  $\mathbf{x}_j$ ,  $j = 1, \dots, N$ , and it was supposed to record the signals  $\{u_s(t, \mathbf{x}_j), t \in [T_j, T_j + \Delta T]\}$  during these successive and disjoint time intervals. Then the Passive Synthetic Aperture (psa) imaging function was proposed:

$$\mathcal{I}_{\text{psa}}(\mathbf{z}^S) = \sum_{j=1}^N \mathcal{C}_{\Delta T, j} (2\mathcal{T}(\mathbf{x}_j, \mathbf{z}^S)), \quad (6)$$

$$\mathcal{C}_{\Delta T, j}(\tau) = \frac{1}{\Delta T} \int_0^{\Delta T} u_s(T_j + t, \mathbf{x}_j) u_s(T_j + t + \tau, \mathbf{x}_j) dt, \quad (7)$$

where  $\mathcal{T}(\mathbf{x}, \mathbf{z})$  is the travel time:

$$\mathcal{T}(\mathbf{x}, \mathbf{z}) = \frac{|\mathbf{x} - \mathbf{z}|}{c_0}. \quad (8)$$

The introduction of the imaging function (6) in [13] was motivated by the relationship between the autocorrelation of the noise signal recorded by the receiver and the Green's function from this receiver to itself [10]. This Green's function has a peak at time equal to twice the travel time from the receiver to the reflector that corresponds to a wave backscattered by the reflector. That is why the autocorrelation  $\mathcal{C}_{\Delta T, j}(\tau)$  of the recorded noise signal is evaluated in (6) at twice the travel time from the receiver position to the search point, in order to capture this peak, and these migrated autocorrelations are summed over the successive time windows. However the analysis carried out in [13] was based on the stop-go approximation (which allows to neglect the Doppler effect) and on an extended source distribution model.

The analysis in [13] shows that the imaging function (6) fails when the spatial distribution of the noise sources is limited. However, when a relatively large time window is used, then the Doppler effect cannot be neglected anymore and it can in fact play a beneficial role to localize the reflector. That is our motivation to introduce the Doppler Passive Synthetic Aperture (dpsa) imaging function as a sum of migrated and Doppler-corrected autocorrelation functions of the recorded signal (2) over successive time windows. It has the form:

$$\mathcal{I}_{\text{dpsa}}(\mathbf{z}^S) = \sum_{j=1}^N \mathcal{I}_{\text{dpsa}, j}(\mathbf{z}^S), \quad (9)$$

$$\begin{aligned} \mathcal{I}_{\text{dpsa}, j}(\mathbf{z}^S) = & \frac{1}{\Delta T} \int_{-\infty}^{\infty} \Pi\left(\frac{t}{\Delta T}\right) U_s\left(T_j + \frac{t}{1 + \beta(T_j, \mathbf{z}^S)}\right) \\ & \times U_s\left(T_j + \frac{t + 2\mathcal{T}(\mathbf{X}(T_j), \mathbf{z}^S)}{1 - \beta(T_j, \mathbf{z}^S)}\right) dt, \end{aligned} \quad (10)$$

where  $\beta(t, \mathbf{z})$  is the Doppler factor:

$$\beta(t, \mathbf{z}) = \frac{\dot{\mathbf{X}}(t)}{c_0} \cdot \frac{\mathbf{X}(t) - \mathbf{z}}{|\mathbf{X}(t) - \mathbf{z}|}, \quad (11)$$

$\dot{\mathbf{X}}(t)$  is the velocity of the receiver antenna at time  $t$ ,  $\Pi(s)$  is a normalized time-window function, we may think at  $\Pi(s) = \mathbf{1}_{[-1/2, 1/2]}(s)$  or  $\Pi(s) = \exp(-s^2/2)$  for instance,  $\Delta T = T/N$  is the width of the time window, and  $T_j = (j - 1/2)\Delta T$ ,  $j = 1, \dots, N$  is the center of  $j$ th recording time window. Note that the recording time intervals are here assumed to be consecutive (if  $\Pi(s) = \mathbf{1}_{[-1/2, 1/2]}(s)$ ) or even overlapping (if  $\Pi(s) = \exp(-s^2/2)$ ) so as to exploit the whole data set generated by the noise sources. The choice of  $\Delta T$  is explained below in Eq. (12). The forms of the Doppler factors come from the analysis of the direct and reflected signals carried out in the following.

Note that we do not need to know anything about the source to compute the imaging function. Up to the Doppler factors  $\beta$ , the imaging function (9) is similar to the imaging function (6) proposed in [13]. In fact, if  $\Pi(s) = \mathbf{1}_{[0, 1]}(s)$  and the displacement of  $\mathbf{X}(t)$

is neglected over the time interval  $[T_j, T_j + \Delta T]$  so that  $\beta(T_j, \mathbf{z}^S) = 0$ , then the two imaging functions (6) and (9) coincide.

The use of Doppler effect in passive synthetic aperture imaging is not new. The authors in the series of papers [23, 24, 26, 27] have developed an approach in which the windowed signal obtained from one receiver is correlated with the scaled and translated version of the received signal in another window from another receiver (or the same one). Only the scattered components of the signals are used and the method requires the opportunistic source to emit the same pulse repeatedly. Here we develop an approach which addresses the case when the noise source emits a stationary random signal. Moreover, we manipulate the total field, that is, the superposition of the scattered field and the direct field, as these components cannot be separated when dealing with stationary random noise sources.

## 2.2. Summary of the main results

We choose a time window  $\Delta T$  such that

$$\max\left(\frac{L}{c_0}, \frac{c_0}{\omega_0 V}\right) \ll \Delta T \ll \sqrt{\frac{\omega_0 L}{c_0}} \frac{c_0}{\omega_0 V}. \quad (12)$$

As we will see below, this means that:

- the time window is longer than the typical travel time  $L/c_0$ ,
- Doppler effects are strong on the time scale of the order of  $\Delta T$ ,
- Doppler effects can be quantitatively captured by expanding the phase terms to first order in  $V/c_0$ .

Note that we should therefore take  $\Delta T \sim 10^{-3}$ – $10^{-2}$ s with the numbers cited above. We will also make use of the assumption that  $BL/c_0 \gg 1$  (i.e., the typical travel time is larger than the pulse width) and  $L \gg V\Delta T$  (i.e., the receiver displacement during one time window is smaller than the range) which is clearly justified in all practical settings. For instance, in our setting,  $L/c_0$  is of the order of  $10^{-4}$ s and  $1/B$  is of the order of  $10^{-8}$ s,  $V\Delta T$  is of the order of 1m and  $L$  is of the order of 10km.

We also assume that the bandwidth  $B$  of the noise sources is such that

$$\frac{1}{\Delta T} \ll B \ll \omega_0. \quad (13)$$

This condition is readily fulfilled in radar configurations.

Finally we also assume a geometric condition, which is that the receiver antenna trajectory is between the source position(s) and the reflector position(s). The exact assumption is the receiver antenna trajectory intersects the segment(s) joining the source position(s) and the reflector position(s). This is the so-called daylight illumination condition that is introduced in particular in [10] in the context of passive imaging with stationary receiver arrays.

Under these circumstances, the imaging function (9) can localize the reflector to the vicinity of the line that goes through  $\mathbf{z}_r$  and is orthogonal to the vector  $\mathbf{z}_r - \mathbf{x}_s$  when there is a single source at  $\mathbf{x}_s$  whose position is unknown. The thickness of this

line (defining the ‘range’ resolution) is of the order of  $c_0/B$ . When there are several well-separated independent noise sources with unknown positions, the reflector can be localized at the intersection of these lines, with a resolution of the order of  $c_0/B$ . The Doppler effect plays a crucial role in this result. It is the Doppler correction in the imaging function that, together with the travel-time migration, gives the localization of the reflector.

When there is a point-like noise source with known position, an alternative imaging function can be used as described in Section 5, that provides a localization of the reflector with a resolution that is equivalent to the one obtained with standard, active synthetic aperture imaging (i.e., when the moving antenna is both a transmitter and a receiver and it emits a train of short pulses with central frequency  $\omega_0$  and bandwidth  $B$ ). In this case, the cross-range resolution is given by the Rayleigh resolution formula  $\lambda_0 L/a$ , where  $\lambda_0$  is the central wavelength of the noise sources,  $a$  is the length of the trajectory of the receiver antenna (during the recording time window  $[0, T]$ ), and  $L$  is the propagation distance from the receiver antenna to the reflector to be imaged. The range resolution is again given by  $c_0/B$ , where  $B$  is the noise source bandwidth.

### 3. Analysis of the imaging function

#### 3.1. The recorded signals

We denote by  $\hat{G}$  the time-harmonic Green’s function for the wave equation with the speed of propagation of the form (1). It is the solution to

$$\frac{\omega^2}{c^2(\mathbf{x})}\hat{G}(\omega, \mathbf{x}, \mathbf{y}) + \Delta_{\mathbf{x}}\hat{G}(\omega, \mathbf{x}, \mathbf{y}) = -\delta(\mathbf{x} - \mathbf{y}), \quad (14)$$

with Sommerfeld radiation condition. The Green’s function satisfies the Lippmann-Schwinger equation,

$$\hat{G}(\omega, \mathbf{x}, \mathbf{y}) = \hat{G}_0(\omega, \mathbf{x}, \mathbf{y}) + \frac{\omega^2}{c_0^2}\sigma_r \int_{\Omega_r} \hat{G}_0(\omega, \mathbf{x}, \mathbf{z})\hat{G}(\omega, \mathbf{z}, \mathbf{y})d\mathbf{z}, \quad (15)$$

where  $\hat{G}_0$  is the Green’s function of the background medium, that is, in the absence of reflector:

$$\frac{\omega^2}{c_0^2}\hat{G}_0(\omega, \mathbf{x}, \mathbf{y}) + \Delta_{\mathbf{x}}\hat{G}_0(\omega, \mathbf{x}, \mathbf{y}) = -\delta(\mathbf{x} - \mathbf{y}). \quad (16)$$

Since we assume that the reflector is weak, we can use the Born (or single-scattering) approximation for the Green’s function:

$$\hat{G}(\omega, \mathbf{x}, \mathbf{y}) = \hat{G}_0(\omega, \mathbf{x}, \mathbf{y}) + \frac{\omega^2}{c_0^2}\sigma_r \int_{\Omega_r} \hat{G}_0(\omega, \mathbf{x}, \mathbf{z})\hat{G}_0(\omega, \mathbf{z}, \mathbf{y})d\mathbf{z}. \quad (17)$$

If, moreover, the reflector has small support (smaller than the typical wavelength), then we get the point-like approximation:

$$\hat{G}(\omega, \mathbf{x}, \mathbf{y}) = \hat{G}_0(\omega, \mathbf{x}, \mathbf{y}) + \frac{\omega^2}{c_0^2}\sigma_r l_r^2 \hat{G}_0(\omega, \mathbf{x}, \mathbf{z}_r)\hat{G}_0(\omega, \mathbf{z}_r, \mathbf{y}). \quad (18)$$

We will use this model for the data. Note that, in a two-dimensional open medium,  $\hat{G}_0$  is the homogeneous Green's function given by

$$\hat{G}_0(\omega, \mathbf{x}, \mathbf{y}) = \frac{i}{4} H_0^{(1)}\left(\frac{\omega}{c_0} |\mathbf{y} - \mathbf{x}|\right), \quad (19)$$

where  $H_0^{(1)}$  is the zeroth order Hankel function of the first kind. Using the asymptotic form of the Hankel function [1, formula 9.2.3], we see that the high-frequency behavior of the homogeneous Green's function is related to the travel time  $|\mathbf{x} - \mathbf{y}|/c_0$ :

$$\hat{G}_0(\omega, \mathbf{x}, \mathbf{y}) \simeq \frac{\sqrt{c_0}}{\sqrt{8\pi\omega|\mathbf{x} - \mathbf{y}|}} \exp\left(i\omega \frac{|\mathbf{x} - \mathbf{y}|}{c_0} + i\frac{\pi}{4}\right). \quad (20)$$

We can write the recorded signal in terms of the homogeneous Green's function as

$$U_s(T_j + t) = U_{sj}^{\text{dir}}(t) + U_{sj}^{\text{sca}}(t), \quad (21)$$

$$U_{sj}^{\text{dir}}(t) = \frac{1}{2\pi} \int_{\mathbb{R}} \hat{n}_s(\omega) \hat{G}_0(\omega, \mathbf{X}(T_j + t), \mathbf{x}_s) e^{-i\omega(T_j+t)} d\omega, \quad (22)$$

$$U_{sj}^{\text{sca}}(t) = \frac{1}{2\pi} \int_{\mathbb{R}} \frac{\omega^2 \sigma_r l_r^2}{c_0^2} \hat{n}_s(\omega) \hat{G}_0(\omega, \mathbf{X}(T_j + t), \mathbf{z}_r) \hat{G}_0(\omega, \mathbf{z}_r, \mathbf{x}_s) e^{-i\omega(T_j+t)} d\omega. \quad (23)$$

**Remark.** If instead of a noise source  $n_s(t)$  at  $\mathbf{x}_s$  we consider an impulsive source emitting the signal  $f_s(t - T_j)$ , then, by using the high-frequency asymptotic form of the homogeneous Green's function and the expansion  $\mathbf{X}(T_j + t) \simeq \mathbf{X}(T_j) + \dot{\mathbf{X}}(T_j)t$ , we can give approximate expressions for the Fourier transforms of the direct and scattered components of the recorded signal:

$$\begin{aligned} \hat{U}_{sj}^{\text{dir}}(\omega) &= \frac{\sqrt{c_0}}{\sqrt{(1 - \beta(T_j, \mathbf{x}_s))8\pi\omega|\mathbf{X}(T_j) - \mathbf{x}_s|}} \hat{f}_s\left(\frac{\omega}{1 - \beta(T_j, \mathbf{x}_s)}\right) \\ &\times \exp\left(i\frac{\omega}{(1 - \beta(T_j, \mathbf{x}_s))c_0} [|\mathbf{X}(T_j) - \mathbf{x}_s|] + i\frac{\pi}{4}\right), \end{aligned} \quad (24)$$

$$\begin{aligned} \hat{U}_{sj}^{\text{sca}}(\omega) &= \frac{\sigma_r l_r^2 \omega}{(1 - \beta(T_j, \mathbf{z}_r))^2 8\pi c_0 \sqrt{|\mathbf{X}(T_j) - \mathbf{z}_r| |\mathbf{z}_r - \mathbf{x}_s|}} \hat{f}_s\left(\frac{\omega}{1 - \beta(T_j, \mathbf{z}_r)}\right) \\ &\times \exp\left(i\frac{\omega}{(1 - \beta(T_j, \mathbf{z}_r))c_0} [|\mathbf{X}(T_j) - \mathbf{z}_r| + |\mathbf{z}_r - \mathbf{x}_s|] + i\frac{\pi}{2}\right). \end{aligned} \quad (25)$$

This allows us to see that each component has a specific Doppler factor. Indeed the direct wave that reaches the receiver comes from  $\mathbf{x}_s$ , hence the Doppler factor  $\beta(T_j, \mathbf{x}_s)$ , while the scattered wave comes from  $\mathbf{z}_r$ , hence the Doppler factor  $\beta(T_j, \mathbf{z}_r)$ . The leading-order corrections due to the Doppler effects appear in the phases of Eqs. (24-25) and are of the form  $\omega\beta L/c_0$ , for some typical travel time  $L/c_0$ . Therefore the Doppler effects for an impulsive source (and only for an impulsive source) can be neglected if  $\omega_0 \frac{L}{c_0} \frac{V}{c_0} \ll 1$ , where  $\omega_0$  is the carrier frequency of the emitted pulse,  $L/c_0$  is the typical travel time, and  $V$  is the velocity of the receiver ( $V/c_0$  is the typical amplitude of the Doppler factor  $\beta$ ). However Eqs. (24-25) will not be used in the following sections and we will see at the end of Subsection 3.3 that the condition  $\omega_0 \frac{L}{c_0} \frac{V}{c_0} \ll 1$  is actually not a sufficient condition to neglect Doppler effects in the case of noise sources.

### 3.2. The imaging function

The partial imaging function (10) is given by

$$\mathcal{I}_{\text{dpsa},j}(\mathbf{z}^S) = \frac{1}{\Delta T} \int_{-\infty}^{\infty} \Pi\left(\frac{t}{\Delta T}\right) U_{sj}^{\text{dir}}\left(\frac{t}{1 + \beta(T_j, \mathbf{z}^S)}\right) U_{sj}^{\text{sca}}\left(\frac{t + 2\mathcal{T}(\mathbf{X}(T_j), \mathbf{z}^S)}{1 - \beta(T_j, \mathbf{z}^S)}\right) dt. \quad (26)$$

There should be three other contributions, namely a term with products  $U_{sj}^{\text{dir}}(\cdot)U_{sj}^{\text{dir}}(\cdot)$ , a term with products  $U_{sj}^{\text{sca}}(\cdot)U_{sj}^{\text{dir}}(\cdot)$ , and a term with product  $U_{sj}^{\text{sca}}(\cdot)U_{sj}^{\text{sca}}(\cdot)$ . However these contributions vanish because they involve the correlation of two pieces of signals emitted by the source for time lags much larger than the coherence time  $1/B$ . We give a detailed proof for the contribution related to  $U_{sj}^{\text{dir}}(\cdot)U_{sj}^{\text{dir}}(\cdot)$  in [Appendix A](#).

**Proposition 3.1** *Under Assumptions (12-13), the partial imaging function (10) has the form*

$$\begin{aligned} \mathcal{I}_{\text{dpsa},j}(\mathbf{z}^S) &= \frac{1}{2^{9/2}\pi^{3/2}} \frac{\sigma_r l_r^2}{\sqrt{|\mathbf{X}(T_j) - \mathbf{z}_r| |\mathbf{z}_r - \mathbf{x}_s| |\mathbf{X}(T_j) - \mathbf{x}_s|}} \\ &\times \frac{\sqrt{i\omega_0}}{\sqrt{c_0}} \exp\left(i\frac{\omega_0}{c_0} (|\mathbf{X}(T_j) - \mathbf{z}_r| + |\mathbf{z}_r - \mathbf{x}_s| - |\mathbf{X}(T_j) - \mathbf{x}_s| - 2|\mathbf{z}^S - \mathbf{X}(T_j)|)\right) \\ &\times F_B\left(-\frac{1}{c_0} (|\mathbf{X}(T_j) - \mathbf{z}_r| + |\mathbf{z}_r - \mathbf{x}_s| - |\mathbf{X}(T_j) - \mathbf{x}_s| - 2|\mathbf{z}^S - \mathbf{X}(T_j)|)\right) \\ &\times \hat{\Pi}\left(\omega_0 \Delta T (\beta(T_j, \mathbf{z}_r) - \beta(T_j, \mathbf{x}_s) - 2\beta(T_j, \mathbf{z}^S))\right) \\ &\times \exp\left(i\frac{\omega_0}{c_0} |\mathbf{X}(T_j) - \mathbf{z}^S| (\beta(T_j, \mathbf{z}_r) - \beta(T_j, \mathbf{z}^S))\right) + cc. \end{aligned} \quad (27)$$

By inspection of the argument of  $\hat{\Pi}$  in Eq. (27), which is of the order of  $\omega_0 \Delta T \beta$  while  $\beta$  is of the order of  $V/c_0$ , we can see that the Doppler effects are important by Assumption (12):  $\omega_0 \Delta T V/c_0 \gg 1$ . Furthermore, if one uses the imaging function (6) instead of (9), then one obtains the same expression as (27), but without the term  $-2\beta(T_j, \mathbf{z}^S)$  in the argument of  $\hat{\Pi}$  and without the term  $-\beta(T_j, \mathbf{z}^S)$  in the argument of the last exponential. Since  $\omega_0 \Delta T \beta \gg 1$  the term in  $\hat{\Pi}$  (that decays very rapidly if  $\Pi$  is smooth) vanishes and the imaging function (6) completely fails.

*Proof.* Using the expressions (22-23) of the direct and scattered components, we find:

$$\begin{aligned} \mathcal{I}_{\text{dpsa},j}(\mathbf{z}^S) &= \frac{1}{(2\pi)^2 \Delta T} \int_{-\infty}^{\infty} \Pi\left(\frac{t}{\Delta T}\right) \int_{\mathbb{R}^2} \overline{\hat{n}_s(\omega')} \hat{G}_0\left(\omega', \mathbf{X}\left(T_j + \frac{t}{1 + \beta(T_j, \mathbf{z}^S)}\right), \mathbf{x}_s\right) \\ &\times \hat{n}_s(\omega) \frac{\omega^2 \sigma_r l_r^2}{c_0^2} \hat{G}_0\left(\omega, \mathbf{X}\left(T_j + \frac{t + 2\mathcal{T}(\mathbf{X}(T_j), \mathbf{z}^S)}{1 - \beta(T_j, \mathbf{z}^S)}\right), \mathbf{z}_r\right) \hat{G}_0(\omega, \mathbf{z}_r, \mathbf{x}_s) \\ &\times \exp\left(i\omega' \left(T_j + \frac{t}{1 + \beta(T_j, \mathbf{z}^S)}\right) - i\omega \left(T_j + \frac{t + 2\mathcal{T}(\mathbf{X}(T_j), \mathbf{z}^S)}{1 - \beta(T_j, \mathbf{z}^S)}\right)\right) d\omega d\omega' dt. \end{aligned} \quad (28)$$

Since  $\Delta T$  is larger than the coherence time of the noise sources, that is,  $B\Delta T \gg 1$ , the autocorrelation function is self-averaging and with the form of its autocorrelation function in the Fourier domain

$$\left\langle \overline{\hat{n}_s(\omega)} \hat{n}_s(\omega') \right\rangle = 2\pi \hat{F}(\omega) \delta(\omega - \omega'), \quad (29)$$

we obtain

$$\begin{aligned}
 \mathcal{I}_{\text{dpsa},j}(\mathbf{z}^S) &= \frac{1}{2\pi\Delta T} \int_{-\infty}^{\infty} \Pi\left(\frac{t}{\Delta T}\right) \int_{\mathbb{R}} \hat{F}(\omega) \overline{\hat{G}_0}\left(\omega, \mathbf{X}\left(T_j + \frac{t}{1 + \beta(T_j, \mathbf{z}^S)}\right), \mathbf{x}_s\right) \\
 &\quad \times \frac{\omega^2 \sigma_r l_r^2}{c_0^2} \hat{G}_0\left(\omega, \mathbf{X}\left(T_j + \frac{t + 2\mathcal{T}(\mathbf{X}(T_j), \mathbf{z}^S)}{1 - \beta(T_j, \mathbf{z}^S)}\right), \mathbf{z}_r\right) \hat{G}_0(\omega, \mathbf{z}_r, \mathbf{x}_s) \\
 &\quad \times \exp\left(i\omega\left(\frac{t}{1 + \beta(T_j, \mathbf{z}^S)} - \frac{t + 2\mathcal{T}(\mathbf{X}(T_j), \mathbf{z}^S)}{1 - \beta(T_j, \mathbf{z}^S)}\right)\right) d\omega dt.
 \end{aligned} \tag{30}$$

From Assumption (12), we have

$$\frac{V}{c_0} \omega_0 \Delta T \gg 1. \tag{31}$$

By inspection of the phase (i.e., the last line) in Eq. (30), we can see that the Doppler correction is of the order of  $\omega t \beta$ . Since  $\omega$  is of the order of  $\omega_0$ ,  $t$  is of the order of  $\Delta T$ , and  $\beta$  is of the order of  $V/c_0$ , we can see that the Doppler effects are important. Since  $\frac{\Delta T c_0}{L} \gg 1$ , we also have  $\frac{V^2}{c_0^2} \omega_0 \Delta T \ll \frac{V^2}{c_0^2} \omega_0 \Delta T \frac{\Delta T c_0}{L} = \frac{V^2}{c_0 L} \omega_0 \Delta T^2$ , which is small by (12). Accordingly,

$$\frac{V^2}{c_0^2} \omega_0 \Delta T \ll 1, \tag{32}$$

so that we can expand the Doppler terms to first-order in  $V/c_0$ . By using the high-frequency asymptotic form (20) of the homogeneous Green's function, we then get

$$\begin{aligned}
 \mathcal{I}_{\text{dpsa},j}(\mathbf{z}^S) &= \frac{1}{2^{11/2} \pi^{5/2}} \frac{\sigma_r l_r^2}{\sqrt{|\mathbf{X}(T_j) - \mathbf{z}_r| |\mathbf{z}_r - \mathbf{x}_s| |\mathbf{X}(T_j) - \mathbf{x}_s|}} \int_{\mathbb{R}} \frac{\sqrt{i\omega}}{\sqrt{c_0}} \hat{F}(\omega) \\
 &\quad \times \exp\left(i\frac{\omega}{c_0} (|\mathbf{X}(T_j) - \mathbf{z}_r| + |\mathbf{z}_r - \mathbf{x}_s| - |\mathbf{X}(T_j) - \mathbf{x}_s| - 2|\mathbf{z}^S - \mathbf{X}(T_j)|)\right) \\
 &\quad \times \hat{\Pi}\left(\omega \Delta T (\beta(T_j, \mathbf{z}_r) - \beta(T_j, \mathbf{x}_s) - 2\beta(T_j, \mathbf{z}^S))\right) \\
 &\quad \times \exp\left(i\frac{\omega}{c_0} |\mathbf{X}(T_j) - \mathbf{z}^S| (\beta(T_j, \mathbf{z}_r) - \beta(T_j, \mathbf{z}^S))\right) d\omega.
 \end{aligned} \tag{33}$$

Using the fact that  $B \ll \omega_0$ , we eventually get the desired result (27).  $\square$

Here we can briefly discuss the behavior of the partial imaging function (10):

- Since  $F_B$  has width  $1/B$ , the third term in the right-hand side of (27) (the term that involves  $F_B$ , and that comes from travel-time migration) imposes that the argument of  $F_B$  should be smaller than  $1/B$ , which means that  $\mathbf{z}^S$  should be in a narrow annulus with center at  $\mathbf{X}(T_j)$ , with radius  $\frac{1}{2}(|\mathbf{X}(T_j) - \mathbf{z}_r| + |\mathbf{z}_r - \mathbf{x}_s| - |\mathbf{X}(T_j) - \mathbf{x}_s|)$ :

$$|\mathbf{z}^S - \mathbf{X}(T_j)| \simeq \frac{1}{2} (|\mathbf{X}(T_j) - \mathbf{z}_r| + |\mathbf{z}_r - \mathbf{x}_s| - |\mathbf{X}(T_j) - \mathbf{x}_s|), \tag{34}$$

and with small width  $c_0/B$ . Note that the radius of the annulus (the right-hand side of (34)) is positive by the triangular inequality.

- Since  $\hat{\Pi}$  has width one, the fourth term in (27) (the term that involves  $\hat{\Pi}$  and that comes from Doppler corrections) imposes that the argument of  $\hat{\Pi}$  should be smaller than

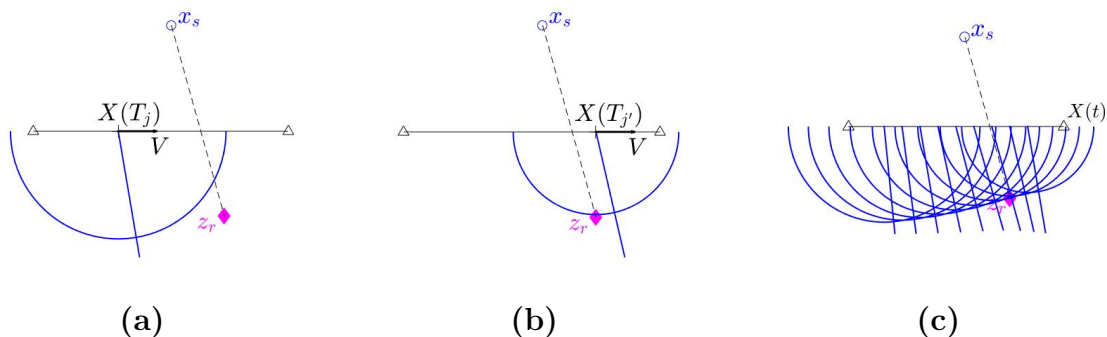


**Figure 2.** The partial imaging function  $\mathcal{I}_{\text{dpsa},j}(\mathbf{z}^S)$  presents a peak at the intersection of the narrow annulus (34) and the narrow cone (35). In pictures (a) and (b) the narrow annulus (represented by half a circle) and the narrow cone (represented by a line) are plotted for two different  $T_j$ 's. In picture (c) they are plotted for a sequence of nine  $T_j$ 's. Here  $\mathbf{x}_s$  is the source position,  $\mathbf{z}_r$  is the reflector position,  $(\mathbf{X}(t))_{t \in [0,T]}$  is the receiver antenna trajectory.

one, which means that the unit vector  $(\mathbf{z}^S - \mathbf{X}(T_j))/|\mathbf{z}^S - \mathbf{X}(T_j)|$  should be in a small angular cone centered along the direction defined by:

$$\frac{\dot{\mathbf{X}}(T_j)}{c_0} \cdot \frac{\mathbf{z}^S - \mathbf{X}(T_j)}{|\mathbf{z}^S - \mathbf{X}(T_j)|} = \frac{1}{2}(\beta(T_j, \mathbf{z}_r) - \beta(T_j, \mathbf{x}_s)), \quad (35)$$

the width of the cone being  $c_0/(V\omega_0\Delta T)$ .

Therefore the partial imaging function  $\mathcal{I}_{\text{dpsa},j}(\mathbf{z}^S)$  has a peak centered at one particular point  $\mathbf{z}_j$ , which is at the intersection of the narrow annulus and the small angular cone that we have just described (see Figure 2). This point is not, in general,  $\mathbf{z}_r$ , as we will see below. But the overall idea is that this point moves as the receiver antenna moves and this motion is essentially ‘stationary’ at the reflector position.

### 3.3. Resolution analysis

In the forthcoming detailed resolution analysis, we assume that the segment joining  $\mathbf{z}_r$  and  $\mathbf{x}_s$  intersects the receiver antenna trajectory in a unique point that we denote by  $\mathbf{X}_s$ . We also denote by  $\mathbf{V}_s$  the velocity vector of the receiver antenna when it is at position  $\mathbf{X}_s$ . We need to assume that the velocity vector of the receiver antenna is approximately constant at the time scale  $c_0L/(V^2\omega_0\Delta T)$ , which is a very reasonable assumption (this time scale is of the order of 1s with the numbers cited above).

We introduce two unit vectors  $\hat{\mathbf{e}}_{s1}, \hat{\mathbf{e}}_{s2}$  that form an orthonormal basis of  $\mathbb{R}^2$ , with

$$\hat{\mathbf{e}}_{s1} = \frac{\mathbf{z}_r - \mathbf{x}_s}{|\mathbf{z}_r - \mathbf{x}_s|}, \quad (36)$$

as shown in Figure 3.

**Proposition 3.2** *Under Assumptions (12-13), the imaging function (9) has the form*

$$\mathcal{I}_{\text{dpsa}}(\mathbf{z}^S) = \frac{1}{2^{7/2}\pi^{1/2}} \frac{\sigma_r l_r^2 \Pi(0)}{(\mathbf{V}_s \cdot \hat{\mathbf{e}}_{s2})^2 \Delta T \sqrt{|\mathbf{X}_s - \mathbf{z}_r| |\mathbf{z}_r - \mathbf{x}_s| |\mathbf{X}_s - \mathbf{x}_s|} \left( \frac{1}{|\mathbf{z}_r - \mathbf{X}_s|} + \frac{1}{|\mathbf{x}_s - \mathbf{X}_s|} \right)} \frac{\sqrt{ic_0}}{\sqrt{\omega_0}}$$

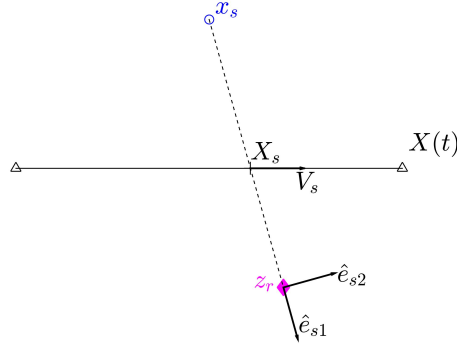


**Figure 3.** Framework for the resolution analysis for the imaging function (9):  $\mathbf{x}_s$  is the source position,  $\mathbf{z}_r$  is the reflector position,  $(\mathbf{X}(t))_{t \in [0, T]}$  is the receiver antenna trajectory,  $\mathbf{X}_s$  and  $\mathbf{V}_s$  are the receiver position and velocity at the critical time when the trajectory crosses the segment joining  $\mathbf{z}_r$  and  $\mathbf{x}_s$ .

$$\begin{aligned}
& \times \exp \left( -i \frac{\omega_0}{c_0} \left( 2\mathbf{y}^S \cdot \hat{\mathbf{e}}_{s1} + \frac{(\mathbf{y}^S \cdot \hat{\mathbf{e}}_{s2})^2}{|\mathbf{z}_r - \mathbf{X}_s|} \left( \frac{|\mathbf{x}_s - \mathbf{X}_s| - |\mathbf{z}_r - \mathbf{X}_s|}{|\mathbf{x}_s - \mathbf{X}_s| + |\mathbf{z}_r - \mathbf{X}_s|} \right) - \mathbf{y}^S \cdot \hat{\mathbf{e}}_{s2} \frac{\hat{\mathbf{e}}_{s2} \cdot \mathbf{V}_s}{c_0} \right) \right) \\
& \times F_B \left( \frac{1}{c_0} \left( 2\mathbf{y}^S \cdot \hat{\mathbf{e}}_{s1} + \frac{(\mathbf{y}^S \cdot \hat{\mathbf{e}}_{s2})^2}{|\mathbf{z}_r - \mathbf{X}_s|} \left( \frac{|\mathbf{x}_s - \mathbf{X}_s| - |\mathbf{z}_r - \mathbf{X}_s|}{|\mathbf{x}_s - \mathbf{X}_s| + |\mathbf{z}_r - \mathbf{X}_s|} \right) - \mathbf{y}^S \cdot \hat{\mathbf{e}}_{s2} \frac{\hat{\mathbf{e}}_{s2} \cdot \mathbf{V}_s}{c_0} \right) \right) \\
& + cc, \tag{37}
\end{aligned}$$

where  $\mathbf{y}^S = \mathbf{z}^S - \mathbf{z}_r$ .

*Proof.* Note that we have  $(\mathbf{z}_r - \mathbf{X}_s)/|\mathbf{z}_r - \mathbf{X}_s| = \hat{\mathbf{e}}_{s1}$  and  $(\mathbf{x}_s - \mathbf{X}_s)/|\mathbf{x}_s - \mathbf{X}_s| = -\hat{\mathbf{e}}_{s1}$  (see Figure 3). By denoting

$$\mathbf{X}(T_j) = \mathbf{X}_s + \delta \mathbf{X}_j \text{ and } \mathbf{z}^S = \mathbf{z}_r + \mathbf{y}^S,$$

we have (up to leading order terms in  $\delta \mathbf{X}_j$  and  $\mathbf{y}^S$ ):

$$\begin{aligned}
|\mathbf{z}^S - \mathbf{X}(T_j)| &= |\mathbf{z}_r - \mathbf{X}_s| + (\mathbf{y}^S - \delta \mathbf{X}_j) \cdot \hat{\mathbf{e}}_{s1} + \frac{(\mathbf{y}^S \cdot \hat{\mathbf{e}}_{s2})^2}{2|\mathbf{z}_r - \mathbf{X}_s|} \\
&\quad - \frac{(\mathbf{y}^S \cdot \hat{\mathbf{e}}_{s2})(\delta \mathbf{X}_j \cdot \hat{\mathbf{e}}_{s2})}{|\mathbf{z}_r - \mathbf{X}_s|} + \frac{(\delta \mathbf{X}_j \cdot \hat{\mathbf{e}}_{s2})^2}{2|\mathbf{z}_r - \mathbf{X}_s|}, \\
|\mathbf{z}_r - \mathbf{X}(T_j)| &= |\mathbf{z}_r - \mathbf{X}_s| - \delta \mathbf{X}_j \cdot \hat{\mathbf{e}}_{s1} + \frac{(\delta \mathbf{X}_j \cdot \hat{\mathbf{e}}_{s2})^2}{2|\mathbf{z}_r - \mathbf{X}_s|}, \\
|\mathbf{x}_s - \mathbf{X}(T_j)| &= |\mathbf{x}_s - \mathbf{X}_s| + \delta \mathbf{X}_j \cdot \hat{\mathbf{e}}_{s1} + \frac{(\delta \mathbf{X}_j \cdot \hat{\mathbf{e}}_{s2})^2}{2|\mathbf{x}_s - \mathbf{X}_s|},
\end{aligned}$$

so that the phase term in (27) can be expanded as

$$\begin{aligned}
& |\mathbf{X}(T_j) - \mathbf{z}_r| + |\mathbf{z}_r - \mathbf{x}_s| - |\mathbf{X}(T_j) - \mathbf{x}_s| - 2|\mathbf{z}^S - \mathbf{X}(T_j)| \\
&= -2\mathbf{y}^S \cdot \hat{\mathbf{e}}_{s1} - \frac{(\mathbf{y}^S \cdot \hat{\mathbf{e}}_{s2})^2}{|\mathbf{z}_r - \mathbf{X}_s|} + \frac{2(\mathbf{y}^S \cdot \hat{\mathbf{e}}_{s2})(\delta \mathbf{X}_j \cdot \hat{\mathbf{e}}_{s2})}{|\mathbf{z}_r - \mathbf{X}_s|} \\
&\quad - \frac{(\delta \mathbf{X}_j \cdot \hat{\mathbf{e}}_{s2})^2}{2} \left( \frac{1}{|\mathbf{z}_r - \mathbf{X}_s|} + \frac{1}{|\mathbf{x}_s - \mathbf{X}_s|} \right).
\end{aligned}$$

The Doppler term in (27) can also be expanded as

$$\begin{aligned} \beta(T_j, \mathbf{z}_r) - \beta(T_j, \mathbf{x}_s) - 2\beta(T_j, \mathbf{z}^S) &= -\frac{(\mathbf{V}_s \cdot \hat{\mathbf{e}}_{s2})(\delta \mathbf{X}_j \cdot \hat{\mathbf{e}}_{s2})}{c_0} \left( \frac{1}{|\mathbf{z}_r - \mathbf{X}_s|} + \frac{1}{|\mathbf{x}_s - \mathbf{X}_s|} \right) \\ &\quad + 2\frac{(\mathbf{V}_s \cdot \hat{\mathbf{e}}_{s2})(\mathbf{y}^S \cdot \hat{\mathbf{e}}_{s2})}{c_0} \frac{1}{|\mathbf{z}_r - \mathbf{X}_s|}, \end{aligned}$$

and finally

$$\beta(T_j, \mathbf{z}_r) - \beta(T_j, \mathbf{z}^S) = \frac{(\mathbf{V}_s \cdot \hat{\mathbf{e}}_{s2})(\mathbf{y}^S \cdot \hat{\mathbf{e}}_{s2})}{c_0} \frac{1}{|\mathbf{z}_r - \mathbf{X}_s|}. \quad (38)$$

By denoting

$$\widetilde{\delta \mathbf{X}}_j = \delta \mathbf{X}_j - \frac{2|\mathbf{x}_s - \mathbf{X}_s|}{|\mathbf{x}_s - \mathbf{X}_s| + |\mathbf{z}_r - \mathbf{X}_s|} \mathbf{y}^S,$$

we can also write:

$$\begin{aligned} |\mathbf{X}(T_j) - \mathbf{z}_r| + |\mathbf{z}_r - \mathbf{x}_s| - |\mathbf{X}(T_j) - \mathbf{x}_s| - 2|\mathbf{z}^S - \mathbf{X}(T_j)| &= -2\mathbf{y}^S \cdot \hat{\mathbf{e}}_{s1} \\ &\quad - \frac{(\mathbf{y}^S \cdot \hat{\mathbf{e}}_{s2})^2}{|\mathbf{z}_r - \mathbf{X}_s|} \left( \frac{|\mathbf{x}_s - \mathbf{X}_s| - |\mathbf{z}_r - \mathbf{X}_s|}{|\mathbf{x}_s - \mathbf{X}_s| + |\mathbf{z}_r - \mathbf{X}_s|} \right) - \frac{(\widetilde{\delta \mathbf{X}}_j \cdot \hat{\mathbf{e}}_{s2})^2}{2} \left( \frac{1}{|\mathbf{z}_r - \mathbf{X}_s|} + \frac{1}{|\mathbf{x}_s - \mathbf{X}_s|} \right), \\ \beta(T_j, \mathbf{z}_r) - \beta(T_j, \mathbf{x}_s) - 2\beta(T_j, \mathbf{z}^S) &= -\frac{(\mathbf{V}_s \cdot \hat{\mathbf{e}}_{s2})(\widetilde{\delta \mathbf{X}}_j \cdot \hat{\mathbf{e}}_{s2})}{c_0} \left( \frac{1}{|\mathbf{z}_r - \mathbf{X}_s|} + \frac{1}{|\mathbf{x}_s - \mathbf{X}_s|} \right). \end{aligned}$$

From Assumption (12) we have

$$\frac{\omega_0 V^2 \Delta T^2}{c_0 L} \ll 1, \quad (39)$$

so that the sum over  $j$  of (27) contains many Doppler terms that are in the support of the function  $\hat{\Pi}$ . This gives the desired result (37). Note that the last term in (27) gives the term in  $-\mathbf{y}^S \cdot \hat{\mathbf{e}}_{s2} \frac{\hat{\mathbf{e}}_{s2} \cdot \mathbf{V}_s}{c_0}$  in (37) because of (38).  $\square$

By Proposition 3.2, the imaging function (9) is nonzero only if the argument in  $F_B$  in Eq. (37) is smaller than  $1/B$  (which is the width of  $F_B$ ). To leading order, this shows that the reflector can be localized in the vicinity of the line going through  $\mathbf{z}_r$  and perpendicular to  $\hat{\mathbf{e}}_{s1}$ :

$$(\mathbf{z}^S - \mathbf{z}_r) \cdot \hat{\mathbf{e}}_{s1} \simeq 0 \quad (40)$$

with a ‘range’ resolution (along  $\hat{\mathbf{e}}_{s1}$ ) equal to  $c_0/B$ . But there is no ‘cross-range’ resolution (along  $\hat{\mathbf{e}}_{s2}$ ).

**Remark.** Eq. (30) shows that the Doppler effects are negligible if

$$\omega_0 \frac{L V}{c_0 c_0} \ll 1 \text{ and } \omega_0 \Delta T \frac{V}{c_0} \ll 1, \quad (41)$$

where  $V$  is the velocity of the receiver antenna and  $L$  the typical propagation distance. If the condition (41) is satisfied, it is equivalent (and therefore sufficient) to use the simplified version (6) or:

$$\mathcal{I}_{\text{psa}}(\mathbf{z}^S) = \frac{1}{\Delta T} \sum_{j=1}^N \int_{-\infty}^{\infty} \Pi\left(\frac{t}{\Delta T}\right) U_s(T_j + t) U_s(T_j + t + 2\mathcal{T}(\mathbf{X}(T_j), \mathbf{z}^S)) dt, \quad (42)$$

as in [13] for instance. But this imaging function cannot localize the reflector. The imaging function is the superposition of the narrow annuli (34) over the different positions  $\mathbf{X}(T_j)$  and is therefore spread out in the search domain.

Note that the condition  $\omega_0 \frac{L}{c_0} \frac{V}{c_0} \ll 1$  is not sufficient to ensure that Doppler effects can be neglected, it is also necessary that  $\omega_0 \Delta T \frac{V}{c_0} \ll 1$ . The situation in which  $\omega_0 \frac{L}{c_0} \frac{V}{c_0} \ll 1$  and  $\omega_0 \Delta T \frac{V}{c_0} \gg 1$  is a situation in which the imaging function (9) can be used and provides localization of the reflector. This situation can be encountered in realistic situations, for instance, with  $\omega_0 = 2\pi 10^9 \text{rad.s}^{-1}$ ,  $L = 10 \text{km}$ , and  $V = 200 \text{m.s}^{-1}$ , we have  $\omega_0 \frac{L}{c_0} \frac{V}{c_0} \sim 10^{-1}$ .

**Remark.** It is possible to get a better ‘cross-range’ resolution when there are several sources as we discuss in the next section.

#### 4. Multiple sources

We here consider the case where there are in fact  $M$  sources, located at  $\mathbf{x}_s$ ,  $s = 1, \dots, M$ . The recorded data is

$$U(t) = u(t, \mathbf{X}(t)) \text{ for } t \in [0, T], \quad (43)$$

where  $u(t, \mathbf{x})$  is the wave field generated by the  $M$  noise sources:

$$\frac{1}{c^2(\mathbf{x})} \frac{\partial^2 u}{\partial t^2} - \Delta_{\mathbf{x}} u = \sum_{s=1}^M n_s(t) \delta(\mathbf{x} - \mathbf{x}_s), \quad (44)$$

with the speed of propagation of the form (1). The source terms  $n_s(t)$ ,  $s = 1, \dots, M$ , are supposed to be independent and identically distributed, with the statistical distribution described in Section 2.1, so that

$$\langle n_s(t) n_{s'}(t') \rangle = F(t - t') \delta_{ss'},$$

where  $\delta$  is here the Kronecker symbol.

We again use the imaging function (9):

$$\begin{aligned} \mathcal{I}_{\text{dpsa}}(\mathbf{z}^S) &= \frac{1}{\Delta T} \sum_{j=1}^N \int_{-\infty}^{\infty} \Pi\left(\frac{t}{\Delta T}\right) U\left(T_j + \frac{t}{1 + \beta(T_j, \mathbf{z}^S)}\right) \\ &\quad \times U\left(T_j + \frac{t + 2\mathcal{T}(\mathbf{X}(T_j), \mathbf{z}^S)}{1 - \beta(T_j, \mathbf{z}^S)}\right) dt. \end{aligned} \quad (45)$$

The recorded data can be expressed as:

$$U(t) = \sum_{s=1}^M U_s(t) \text{ for } t \in [0, T],$$

where  $U_s(t) = u_s(t, \mathbf{X}(t))$  is the component of the recorded signal that has been emitted by the source at  $\mathbf{x}_s$ , as introduced in (2). Accordingly

$$\mathcal{I}_{\text{dpsa}}(\mathbf{z}^S) = \frac{1}{\Delta T} \sum_{s,s'=1}^M \sum_{j=1}^N \int_{-\infty}^{\infty} \Pi\left(\frac{t}{\Delta T}\right) U_s\left(T_j + \frac{t}{1 + \beta(T_j, \mathbf{z}^S)}\right)$$

$$\times U_{s'}\left(T_j + \frac{t + 2\mathcal{T}(\mathbf{X}(T_j), \mathbf{z}^S)}{1 - \beta(T_j, \mathbf{z}^S)}\right) dt.$$

Each term of this double sum (in  $s, s'$ ) can be analyzed following the lines of the previous sections, and we find that the crossed terms  $s \neq s'$  cancel by independence of the different noise sources. Therefore the imaging function is equal to

$$\begin{aligned} \mathcal{I}_{\text{dpsa}}(\mathbf{z}^S) &= \frac{1}{\Delta T} \sum_{s=1}^M \sum_{j=1}^N \int_{-\infty}^{\infty} \Pi\left(\frac{t}{\Delta T}\right) U_s\left(T_j + \frac{t}{1 + \beta(T_j, \mathbf{z}^S)}\right) \\ &\quad \times U_s\left(T_j + \frac{t + 2\mathcal{T}(\mathbf{X}(T_j), \mathbf{z}^S)}{1 - \beta(T_j, \mathbf{z}^S)}\right) dt. \end{aligned} \quad (46)$$

If the sources are dense and well distributed, then the analysis carried out in [13] can be readily extended to incorporate the Doppler effect and we will find the same result: the ‘range’ resolution is of order  $c_0/B$  and the ‘cross-range’ resolution is of order  $\lambda_0 VT/L$ , where  $VT$  is the length of the trajectory. It turns out that the analysis carried out in this paper shows that we do not need the sources to be dense in order to achieve such a result. Indeed the imaging function is the superposition of the imaging functions studied in the previous sections corresponding to the individual point-like sources. A few sources that produce unit vectors  $\hat{\mathbf{e}}_{s1}$ ,  $s = 1, \dots, M$ , as defined by (36), covering a cone of angular radius of order one will allow to localize the reflector with a ‘range’ and ‘cross-range’ resolution of order  $c_0/B$ . We will see in Section 6 that two well-separated sources are sufficient for reflector localization: the reflector location can be found at the intersection of the two lines  $(\mathbf{z}^S - \mathbf{z}_r) \cdot \hat{\mathbf{e}}_{s1} = 0$ ,  $s = 1, 2$ . Finally, we can remark that the receiver does not need to be coherent on a scale much larger than twice the travel time to the search point, as the autocorrelation is only evaluated for such time lags.

## 5. Single source with known position

We have seen that the imaging function (9) can only localize the reflector to the vicinity of a line when there is a single point-like noise source. This imaging function does not require to know anything about the noise source. If, however, the location  $\mathbf{x}_s$  of the noise source is known, then it is possible to design another imaging function that will be able to localize the reflector accurately. We introduce

$$\mathcal{I}(\mathbf{z}^S) = \sum_{j=1}^N \mathcal{I}_j(\mathbf{z}^S), \quad (47)$$

$$\begin{aligned} \mathcal{I}_j(\mathbf{z}^S) &= \frac{1}{\Delta T} \int_{-\infty}^{\infty} \Pi\left(\frac{t}{\Delta T}\right) U_s\left(T_j + \frac{t}{1 - \beta(T_j, \mathbf{x}_s)}\right) \\ &\quad \times U_s\left(T_j + \frac{t + \mathcal{T}(\mathbf{x}_s, \mathbf{z}^S) + \mathcal{T}(\mathbf{z}^S, \mathbf{X}(T_j)) - \mathcal{T}(\mathbf{x}_s, \mathbf{X}(T_j))}{1 - \beta(T_j, \mathbf{z}^S)}\right) dt. \end{aligned} \quad (48)$$

Here we use the same notations as in Subsection 2.1. Note that we need to know the source position  $\mathbf{x}_s$  to compute this imaging function. Proceeding as in Subsection 3.2,

we obtain that

$$\begin{aligned} \mathcal{I}_j(\mathbf{z}^S) &= \frac{1}{2^{11/2}\pi^{5/2}} \frac{\sigma_r l_r^2}{\sqrt{|\mathbf{X}(T_j) - \mathbf{z}_r| |\mathbf{z}_r - \mathbf{x}_s| |\mathbf{X}(T_j) - \mathbf{x}_s|}} \int_{\mathbb{R}} \frac{\sqrt{i\omega}}{\sqrt{c_0}} \hat{F}(\omega) \\ &\quad \times \exp\left(i\frac{\omega}{c_0} (|\mathbf{X}(T_j) - \mathbf{z}_r| + |\mathbf{z}_r - \mathbf{x}_s| - |\mathbf{z}^S - \mathbf{x}_s| - |\mathbf{X}(T_j) - \mathbf{z}^S|)\right) \\ &\quad \times \exp\left(i\frac{\omega}{c_0} (\beta(T_j, \mathbf{z}_r) - \beta(T_j, \mathbf{z}^S)) (|\mathbf{x}_s - \mathbf{z}^S| + |\mathbf{z}^S - \mathbf{X}(T_j)| - |\mathbf{x}_s - \mathbf{X}(T_j)|)\right) \\ &\quad \times \hat{\Pi}\left(\omega \Delta T (\beta(T_j, \mathbf{z}_r) - \beta(T_j, \mathbf{z}^S))\right) d\omega. \end{aligned} \quad (49)$$

Using the fact that  $B \ll \omega_0$ , we have

$$\begin{aligned} \mathcal{I}_j(\mathbf{z}^S) &= \frac{1}{2^{9/2}\pi^{3/2}} \frac{\sigma_r l_r^2}{\sqrt{|\mathbf{X}(T_j) - \mathbf{z}_r| |\mathbf{z}_r - \mathbf{x}_s| |\mathbf{X}(T_j) - \mathbf{x}_s|}} \\ &\quad \times \frac{\sqrt{i\omega_0}}{\sqrt{c_0}} \exp\left(i\frac{\omega_0}{c_0} (|\mathbf{X}(T_j) - \mathbf{z}_r| + |\mathbf{z}_r - \mathbf{x}_s| - |\mathbf{z}^S - \mathbf{x}_s| - |\mathbf{X}(T_j) - \mathbf{z}^S|)\right) \\ &\quad \times F_B\left(-\frac{1}{c_0} (|\mathbf{X}(T_j) - \mathbf{z}_r| + |\mathbf{z}_r - \mathbf{x}_s| - |\mathbf{z}^S - \mathbf{x}_s| - |\mathbf{X}(T_j) - \mathbf{z}^S|)\right) \\ &\quad \times \exp\left(i\frac{\omega_0}{c_0} (\beta(T_j, \mathbf{z}_r) - \beta(T_j, \mathbf{z}^S)) (|\mathbf{x}_s - \mathbf{z}^S| + |\mathbf{z}^S - \mathbf{X}(T_j)| - |\mathbf{x}_s - \mathbf{X}(T_j)|)\right) \\ &\quad \times \hat{\Pi}\left(\omega_0 \Delta T (\beta(T_j, \mathbf{z}_r) - \beta(T_j, \mathbf{z}^S))\right) + cc. \end{aligned} \quad (50)$$

By writing the search point  $\mathbf{z}^S = \mathbf{z}_r + \mathbf{y}^S$ , we can expand the phase term as

$$\begin{aligned} &|\mathbf{X}(T_j) - \mathbf{z}_r| + |\mathbf{z}_r - \mathbf{x}_s| - |\mathbf{z}^S - \mathbf{x}_s| - |\mathbf{X}(T_j) - \mathbf{z}^S| \\ &= -\mathbf{y}^S \cdot \left( \frac{\mathbf{z}_r - \mathbf{x}_s}{|\mathbf{z}_r - \mathbf{x}_s|} + \frac{\mathbf{z}_r - \mathbf{X}(T_j)}{|\mathbf{z}_r - \mathbf{X}(T_j)|} \right), \end{aligned}$$

and the Doppler term as

$$\begin{aligned} &\beta(T_j, \mathbf{z}_r) - \beta(T_j, \mathbf{z}^S) \\ &= \frac{\dot{\mathbf{X}}(T_j)}{c_0} \cdot \left( \frac{\mathbf{y}^S}{|\mathbf{z}_r - \mathbf{X}(T_j)|} - (\mathbf{z}_r - \mathbf{X}(T_j)) \frac{(\mathbf{z}_r - \mathbf{X}(T_j)) \cdot \mathbf{y}^S}{|\mathbf{z}_r - \mathbf{X}(T_j)|^3} \right). \end{aligned}$$

We assume for simplicity that the antenna trajectory is straight with constant velocity vector  $\mathbf{V}$ . We denote

$$\mathbf{X}_0 = \mathbf{X}(T/2), \quad \Delta \mathbf{X} = \mathbf{X}(T) - \mathbf{X}(0) = \mathbf{V}T, \quad \hat{\mathbf{e}}_s = \frac{\mathbf{z}_r - \mathbf{x}_s}{|\mathbf{z}_r - \mathbf{x}_s|}. \quad (51)$$

We introduce the orthonormal basis  $(\hat{\mathbf{e}}_1, \hat{\mathbf{e}}_2)$  with

$$\hat{\mathbf{e}}_1 = \frac{\mathbf{z}_r - \mathbf{X}_0}{|\mathbf{z}_r - \mathbf{X}_0|}, \quad (52)$$

as shown in Figure 4.

### 5.1. Small-aperture resolution analysis

Here we study the situation when  $|\Delta \mathbf{X}| \ll L$  (i.e. the antenna trajectory is shorter than the propagation distance). We can then write

$$\mathcal{I}(\mathbf{z}^S) = \frac{1}{2^{9/2}\pi^{3/2}} \frac{N\sigma_r l_r^2}{\sqrt{|\mathbf{z}_r - \mathbf{x}_s| |\mathbf{X}_0 - \mathbf{x}_s| |\mathbf{X}_0 - \mathbf{z}_r|}}$$

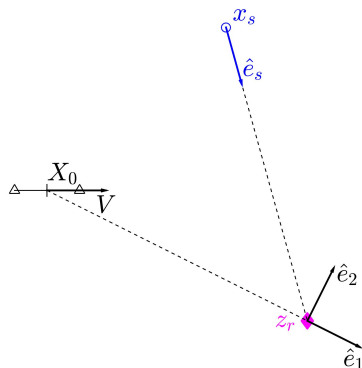


**Figure 4.** Framework for the resolution analysis for the imaging function (47).

$$\begin{aligned} & \times \frac{\sqrt{i\omega_0}}{\sqrt{c_0}} \exp\left(-i\frac{\omega_0}{c_0}\mathbf{y}^S \cdot (\hat{\mathbf{e}}_1 + \hat{\mathbf{e}}_s)\right) F_B\left(\frac{1}{c_0}\mathbf{y}^S \cdot (\hat{\mathbf{e}}_1 + \hat{\mathbf{e}}_s)\right) \\ & \times \text{sinc}\left(\frac{\omega_0}{c_0} \frac{\Delta\mathbf{X} \cdot \hat{\mathbf{e}}_2}{2} \frac{\mathbf{y}^S \cdot \hat{\mathbf{e}}_2}{|\mathbf{z}_r - \mathbf{X}_0|}\right) \hat{\Pi}\left(\omega_0 \frac{\mathbf{V} \cdot \hat{\mathbf{e}}_2 \Delta T}{c_0} \frac{\mathbf{y}^S \cdot \hat{\mathbf{e}}_2}{|\mathbf{z}_r - \mathbf{X}_0|}\right) + cc. \end{aligned} \quad (53)$$

Remember that, in the previous section, we had kept the second-order terms in  $\mathbf{y}^S$  because they were the leading-order terms in the second direction  $\hat{\mathbf{e}}_{s2}$ . Here there are first-order terms in both directions, therefore the second-order terms do not play any role anymore. Since  $\Delta\mathbf{X} \cdot \hat{\mathbf{e}}_2 = \mathbf{V} \cdot \hat{\mathbf{e}}_2 T = N\mathbf{V} \cdot \hat{\mathbf{e}}_2 \Delta T$ , the last term (in  $\hat{\Pi}$ ) is negligible compared to the sinc term, and we find

$$\begin{aligned} \mathcal{I}(\mathbf{z}^S) &= \frac{1}{2^{9/2}\pi^{3/2}} \frac{N\sigma_r l_r^2 \hat{\Pi}(0)}{\sqrt{|\mathbf{z}_r - \mathbf{x}_s| |\mathbf{X}_0 - \mathbf{x}_s| |\mathbf{X}_0 - \mathbf{z}_r|}} \frac{\sqrt{i\omega_0}}{\sqrt{c_0}} \exp\left(-i\frac{\omega_0}{c_0}\mathbf{y}^S \cdot (\hat{\mathbf{e}}_1 + \hat{\mathbf{e}}_s)\right) \\ & \times F_B\left(\frac{1}{c_0}\mathbf{y}^S \cdot (\hat{\mathbf{e}}_1 + \hat{\mathbf{e}}_s)\right) \text{sinc}\left(\frac{\omega_0}{2} \frac{\mathbf{V} \cdot \hat{\mathbf{e}}_2 T}{c_0} \frac{\mathbf{y}^S \cdot \hat{\mathbf{e}}_2}{|\mathbf{z}_r - \mathbf{X}_0|}\right) + cc. \end{aligned} \quad (54)$$

This expression shows that the Doppler effect has been completely mitigated. The resolution of the imaging function (47) in the ‘range’ direction  $\hat{\mathbf{e}}_1$  is equal to  $c_0/(2B \cos^2(\phi_s/2))$ , where  $\phi_s$  is the angle between  $\hat{\mathbf{e}}_1$  and  $\hat{\mathbf{e}}_s$ :  $\cos(\phi_s) = \hat{\mathbf{e}}_1 \cdot \hat{\mathbf{e}}_s$ . The resolution in the ‘cross-range’ direction  $\hat{\mathbf{e}}_2$  is  $L\lambda_0/(\mathbf{V} \cdot \hat{\mathbf{e}}_2 T)$ . These resolution formulas are in agreement with the ones obtained in the usual synthetic aperture imaging when the moving receiver antenna is also a transmitter with the stop-go approximation [7, 8]. This shows that one can get the same images with active and passive imaging provided the source position is known.

## 5.2. Large-aperture resolution analysis

Here we study the situation when  $|\Delta\mathbf{X}| \sim L$  (i.e. the length of the antenna trajectory is of the same order as the propagation distance). The imaging function (47) takes the form

$$\mathcal{I}(\mathbf{z}^S) = \frac{1}{2^{9/2}\pi^{3/2}} \frac{N\sigma_r l_r^2}{\sqrt{|\mathbf{z}_r - \mathbf{x}_s|}} \frac{\sqrt{i\omega_0}}{\sqrt{c_0}} \exp\left(-i\frac{\omega_0}{c_0}\mathbf{y}^S \cdot \hat{\mathbf{e}}_s\right) F_B\left(\frac{1}{c_0}\mathbf{y}^S \cdot (\hat{\mathbf{e}}_1 + \hat{\mathbf{e}}_s)\right)$$

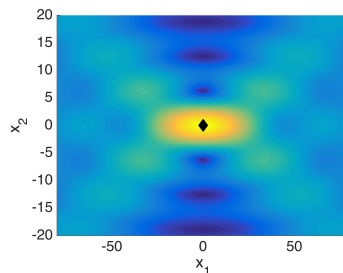


**Figure 5.** Modulus of the normalized point spread function (59).

$$\times \frac{1}{T} \int_0^T \frac{1}{\sqrt{|\mathbf{X}(t) - \mathbf{x}_s| |\mathbf{X}(t) - \mathbf{z}_r|}} \exp\left(-i \frac{\omega_0}{c_0} \mathbf{y}^S \cdot \hat{\mathbf{e}}(t)\right) dt + cc, \quad (55)$$

where

$$\hat{\mathbf{e}}(t) = \frac{\mathbf{z}_r - \mathbf{X}(t)}{|\mathbf{z}_r - \mathbf{X}(t)|}. \quad (56)$$

Since  $B \ll \omega_0$ , the term in  $F_B$  plays a negligible role compared to the last (integral) term:

$$\begin{aligned} \mathcal{I}(\mathbf{z}^S) &= \frac{1}{2^{9/2} \pi^{3/2}} \frac{N \sigma_r l_r^2}{\sqrt{|\mathbf{z}_r - \mathbf{x}_s|}} \frac{\sqrt{i \omega_0}}{\sqrt{c_0}} \exp\left(-i \frac{\omega_0}{c_0} \mathbf{y}^S \cdot \hat{\mathbf{e}}_s\right) \\ &\times \frac{1}{T} \int_0^T \frac{1}{\sqrt{|\mathbf{X}(t) - \mathbf{x}_s| |\mathbf{X}(t) - \mathbf{z}_r|}} \exp\left(-i \frac{\omega_0}{c_0} \mathbf{y}^S \cdot \hat{\mathbf{e}}(t)\right) dt + cc, \end{aligned} \quad (57)$$

and the resolution of the imaging function (47) is determined by the angular cone described by the set of unit vectors  $\{\hat{\mathbf{e}}(t), t \in [0, T]\}$ . If the width of this cone is not too large, then the previous expression can be approximated by the following one (by expanding  $\hat{\mathbf{e}}(t)$  around  $\hat{\mathbf{e}}(T/2) = \hat{\mathbf{e}}_1$ ):

$$\begin{aligned} \mathcal{I}(\mathbf{z}^S) &= \frac{1}{2^{9/2} \pi^{3/2}} \frac{N \sigma_r l_r^2}{\sqrt{|\mathbf{z}_r - \mathbf{x}_s| |\mathbf{X}_0 - \mathbf{x}_s| |\mathbf{X}_0 - \mathbf{z}_r|}} \frac{\sqrt{i \omega_0}}{\sqrt{c_0}} \exp\left(-i \frac{\omega_0}{c_0} \mathbf{y}^S \cdot (\hat{\mathbf{e}}_1 + \hat{\mathbf{e}}_s)\right) \\ &\times \Phi\left(\frac{\omega_0}{c_0} \frac{(\mathbf{V} \cdot \hat{\mathbf{e}}_2 T)^2 + 2(\mathbf{V} \cdot \hat{\mathbf{e}}_1 T)^2}{|\mathbf{z}_r - \mathbf{X}_0|^2} (\mathbf{y}^S \cdot \hat{\mathbf{e}}_1), \frac{\omega_0}{c_0} \frac{\mathbf{V} \cdot \hat{\mathbf{e}}_2 T}{|\mathbf{z}_r - \mathbf{X}_0|} (\mathbf{y}^S \cdot \hat{\mathbf{e}}_2)\right) + cc, \end{aligned} \quad (58)$$

with the normalized point spread function

$$\Phi(x_1, x_2) = \int_{-1/2}^{1/2} \exp\left(i \frac{s^2}{2} x_1 + i s x_2\right) ds. \quad (59)$$

The marginal functions are  $\Phi(x_1, 0) = (C(\sqrt{x_1/8}) + iS(\sqrt{x_1/8}))/\sqrt{x_1/8}$  and  $\Phi(0, x_2) = \text{sinc}(x_2/2)$ , where  $C$  and  $S$  are the tabulated Fresnel integrals [1, Section 7.3]:

$$C(x) = \int_0^x \cos(s^2) ds, \quad S(x) = \int_0^x \sin(s^2) ds.$$

This shows that the width of the normalized point spread function is about  $16\pi$  in the first direction and about  $2\pi$  in the second direction (see Figure 5). Accordingly, when

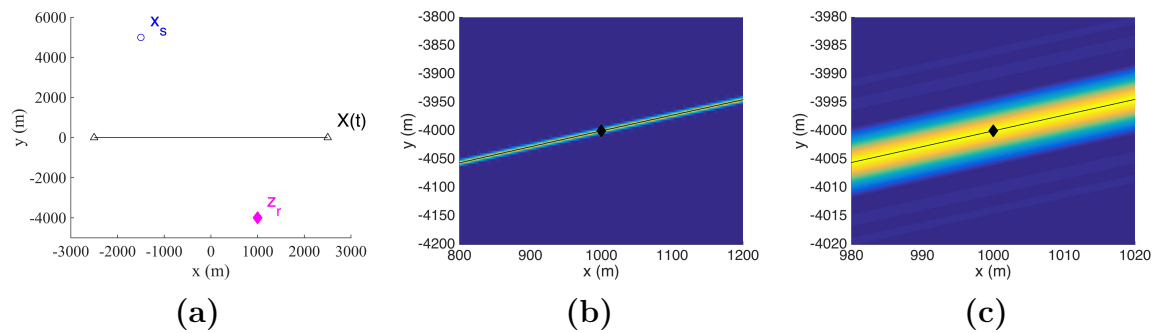


**Figure 6.** Passive sensor array imaging with one unknown source. In picture (a) the geometric set-up is plotted:  $\mathbf{x}_s$  is the source position,  $\mathbf{z}_r$  is the reflector position,  $(\mathbf{X}(t))_{t \in [0, T]}$  is the receiver antenna trajectory. In picture (b) the (modulus of the) imaging function (9) is plotted. The diamond stands for the true position of the reflector, the thin solid line is the theoretical line (40). Picture (c) is a zoom of picture (b).

$\mathbf{V}$  is essentially along  $\hat{\mathbf{e}}_2$ , the resolution of the imaging function in the ‘cross-range’ direction  $\hat{\mathbf{e}}_2$  is  $\lambda_0/\Delta\theta$ , where  $\Delta\theta$  is the width of the angular cone formed by the unit vectors  $\{\hat{\mathbf{e}}(t), t \in [0, T]\}$ :  $\Delta\theta = \mathbf{V} \cdot \hat{\mathbf{e}}_2 T / |\mathbf{z}_r - \mathbf{X}_0|$ . The resolution of the imaging function in the ‘range’ direction  $\hat{\mathbf{e}}_1$  is  $8\lambda_0/\Delta\theta^2$ . These formulas are again in agreement with the corresponding ones in active synthetic aperture imaging.

## 6. Numerical illustrations

### 6.1. Single unknown source

In this subsection we consider the situation in which the illumination is provided by a single unknown point-like noise source. The imaging function (9) is used to localize the reflector at  $\mathbf{z}_r$ . We actually plot the expected value of the imaging function (9) using the expression (30). A full numerical validation of the method would be required with a realistic noise model but it is beyond the scope of this paper. Here the envelope of the power spectral density is Gaussian  $F_B(t) = \exp(-B^2 t^2/2)$ , the time-window function is  $\Pi(s) = \exp(-s^2/2)$ ,  $\omega_0 = 2\pi 10^{10} \text{rad.s}^{-1}$ ,  $B = 2\pi 10^7 \text{rad.s}^{-1}$ ,  $c_0 = 3 \cdot 10^8 \text{m.s}^{-1}$ ,  $\mathbf{V} = (200, 0) \text{m.s}^{-1}$ ,  $\mathbf{X}(0) = (-2500, 0) \text{m}$ ,  $\mathbf{X}(T) = (2500, 0) \text{m}$ ,  $T = 25 \text{s}$ ,  $\Delta T = 0.01 \text{s}$ ,  $\mathbf{z}_r = (1000, -4000) \text{m}$ , and  $\mathbf{x}_s = (-1500, 5000) \text{m}$ . As can be seen in Figure 6(c), the ‘range’ resolution is  $c_0/B \simeq 5 \text{m}$ , but there is no ‘cross-range’ resolution.

### 6.2. Multiple unknown sources

In this subsection we consider the situation in which the illumination is provided by two unknown point-like noise sources. The imaging function (9) (or (45)) is used to localize the reflector at  $\mathbf{z}_r$ . The set-up is similar to the one of the previous subsection, except that there are two point-like noise sources at  $\mathbf{x}_1 = (-1500, 5000) \text{m}$  and  $\mathbf{x}_2 = (1500, 4000) \text{m}$  emitting two independent and identically distributed noise signals. As seen in Figure 7,

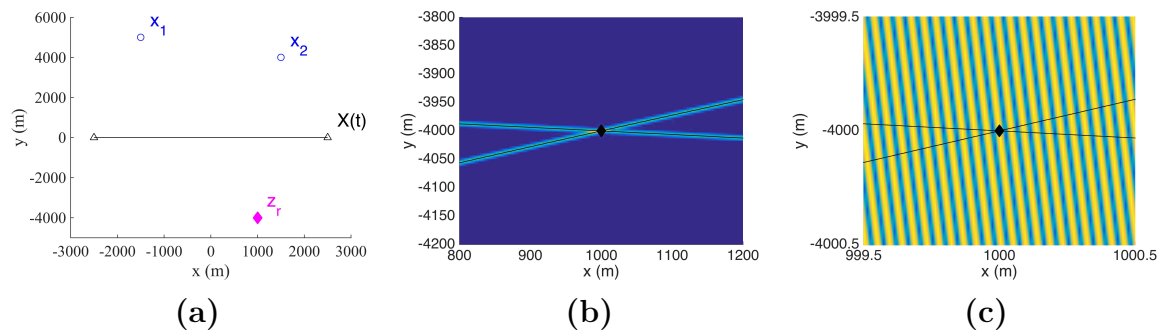


**Figure 7.** Passive sensor array imaging with two unknown sources. In picture (a) the geometric set-up is plotted. In picture (b) the (modulus of the) imaging function (9) is plotted. The diamond stands for the true position of the reflector, the thin solid lines are the theoretical lines (40) for the two sources. Picture (c) is a zoom of picture (b).

the reflector can be localized at the intersection of the two lines (40) with an accuracy of the order of  $c_0/B$ . The fringes that can be seen in the zoom of Figure 7(c) come from the interference of the modulations at the central frequency, they are approximately of the form  $\cos [(\omega_0/c_0)(\hat{e}_{11} - \hat{e}_{21}) \cdot (\mathbf{z}^S - \mathbf{z}_r)]$ , where the vector

$$\hat{e}_{11} - \hat{e}_{21} = \frac{\mathbf{z}_r - \mathbf{x}_1}{|\mathbf{z}_r - \mathbf{x}_1|} - \frac{\mathbf{z}_r - \mathbf{x}_2}{|\mathbf{z}_r - \mathbf{x}_2|},$$

is here equal to  $(0.33, 0.035)$ .

### 6.3. Single known source

In this subsection we consider the situation in which the illumination is provided by a single point-like noise source with known position. The set-up is similar to the one of Subsection 6.1, except that the source position is known so that we can use the imaging function (47) to localize the reflector at  $\mathbf{z}_r$ .

In Figures 8 and 9 we plot the images obtained from two time subwindows  $[0, T_0]$  and  $[T - T_0, T]$ , with  $T_0 = 2.5$ s (the corresponding trajectories of the receiver antenna can be seen in Figures 8(a) and 9(a)). We can see in Figures 8(b) and 9(b) that the resolution in the ‘range’ direction is still  $c_0/B \simeq 5$ m, but the resolution in the ‘cross-range’ direction is now much higher than with the imaging function (9), of the order of  $\lambda_0 L / (VT_0) \simeq 0.5$ m, and secondary lobes corresponding to the sinc function in (54) are visible. Of course, by the use of an apodization function  $\Psi$  with support in  $[0, 1]$  in the sum over  $j$  (such as the Hanning function  $\Psi(s) = \sin^2(\pi s)\mathbf{1}_{[0,1]}(s)$ ):

$$\mathcal{I}(\mathbf{z}^S) = \sum_{j=1}^N \mathcal{I}_j(\mathbf{z}^S) \Psi\left(\frac{j-1}{N-1}\right), \quad (60)$$

it is possible to reduce the secondary lobes (see Figures 8(c) and 9(c)).

Finally, in Figure 10 we plot the image obtained from the full time window  $[0, T]$  (the corresponding trajectory of the receiver antenna can be seen in Figure 10(a)). Note

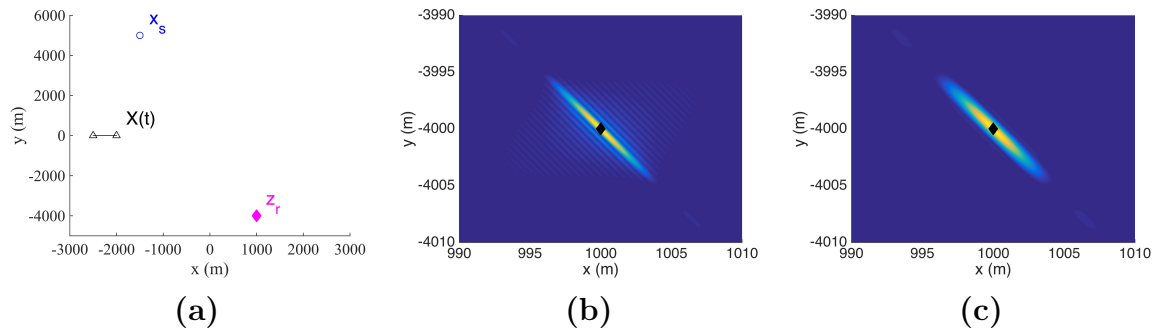


**Figure 8.** Passive sensor array imaging with one known source. In picture (a) the geometric set-up is plotted. In picture (b) the (modulus of the) imaging function (47) is plotted. The diamond stands for the true position of the reflector. In picture (c) the (modulus of the) imaging function (60) with the Hanning function  $\Psi(s) = \sin^2(\pi s)\mathbf{1}_{[0,1]}(s)$ .

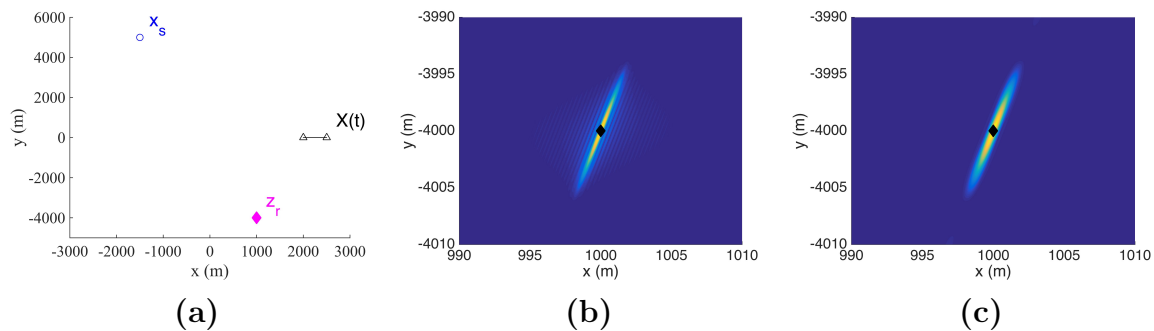


**Figure 9.** Passive sensor array imaging with one known source. In picture (a) the geometric set-up is plotted. In picture (b) the (modulus of the) imaging function (47) is plotted. The diamond stands for the true position of the reflector. In picture (c) the (modulus of the) imaging function (60) with the Hanning function  $\Psi(s) = \sin^2(\pi s)\mathbf{1}_{[0,1]}(s)$ .

that the scales are different compared to the previous figures. We can see that the ‘cross-range’ resolution is about  $\lambda_0 \simeq 0.03\text{m}$  and the ‘range’ resolution is about  $8\lambda_0 \simeq 0.25\text{m}$ , as predicted by the theory for such an aperture.

## 7. Conclusion

In this paper we have analyzed passive synthetic aperture imaging when the illumination is poor and the number of noise sources is very limited. The imaging function uses the autocorrelation functions of the signals recorded by the moving receiver antenna and computed over successive time windows and migrate them with Doppler corrective factors. Qualitatively, the use of rather large time windows enhances the Doppler effect and is profitable for reflector imaging. Quantitatively, we have analyzed in detail a two-dimensional situation and we have shown that the resolution properties of the proposed

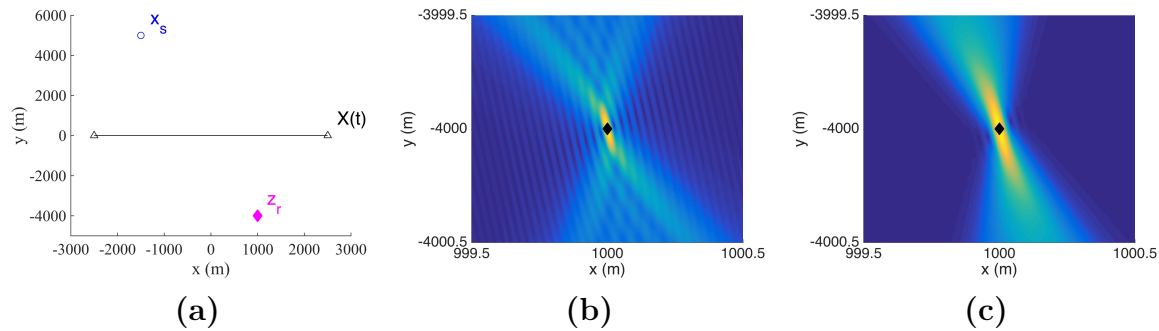


**Figure 10.** Passive sensor array imaging with one known source. In picture (a) the geometric set-up is plotted. In picture (b) the (modulus of the) imaging function (47) is plotted. The diamond stands for the true position of the reflector. In picture (c) the (modulus of the) imaging function (60) with the Hanning function  $\Psi(s) = \sin^2(\pi s)\mathbf{1}_{[0,1]}(s)$ .

imaging functions are the following ones:

- When there is only one point-like noise source, only the range coordinate of the target can be determined with a resolution proportional to the inverse of the noise bandwidth if the position of the source is not known.
- When there is only one point-like noise source whose position is known, then it is possible to get an image with the same resolution properties of the ones of standard active synthetic aperture imaging.
- When there are several (ie, at least two) unknown point-like noise sources that are far from each other, the target can be imaged with an overall resolution proportional to the inverse of the noise bandwidth.

The proposed correlation-based imaging method is robust with respect to measurement noise as it evaluates the correlation of the recorded signals for quite large time lags. It is sensitive to the knowledge of the positions of the receivers. The generalization of the results to a general three-dimensional set-up requires some further work. We may anticipate that we should need at least three unknown sources to localize a reflector in a three-dimensional set-up or two known sources.

In this paper we have focused our attention on reflector localization and we have carried out a resolution analysis. It is possible to improve the quantitative properties of the imaging function by adding a multiplicative factor in the imaging function that compensates for the geometric decay of the Green's function, or more generally by the use of a filter that makes the amplitude of the point spread function independent of the position of the reflector, similarly to [24]. This would allow to address more complex reflectivities as in [4].

## Acknowledgements

The author thanks Liliana Borcea (University of Michigan), George Papanicolaou (Stanford University), Knut Sølna (UC Irvine), and Chrysoula Tsogka (University of Crete) for stimulating discussions.

## Appendix A. The contribution of the direct waves

The partial imaging function (10) has a contribution which comes from the autocorrelation of the direct signals given by

$$\mathcal{I}_{\text{dpsa},j}(\mathbf{z}^S) = \frac{1}{\Delta T} \int_{-\infty}^{\infty} \Pi\left(\frac{t}{\Delta T}\right) U_{sj}^{\text{dir}}\left(\frac{t}{1 + \beta(T_j, \mathbf{z}^S)}\right) U_{sj}^{\text{dir}}\left(\frac{t + 2\mathcal{T}(\mathbf{X}(T_j), \mathbf{z}^S)}{1 - \beta(T_j, \mathbf{z}^S)}\right) dt. \quad (\text{A.1})$$

Using the expression (22) of  $U_{sj}^{\text{dir}}$ , we get:

$$\begin{aligned} \mathcal{I}_{\text{dpsa},j}(\mathbf{z}^S) &= \frac{1}{(2\pi)^2 \Delta T} \int_{-\infty}^{\infty} \Pi\left(\frac{t}{\Delta T}\right) \int_{\mathbb{R}^2} \overline{\hat{n}_s(\omega)} \overline{\hat{G}_0}\left(\omega, \mathbf{X}\left(T_j + \frac{t}{1 + \beta(T_j, \mathbf{z}^S)}\right), \mathbf{x}_s\right) \\ &\quad \times \hat{n}_s(\omega') \hat{G}_0\left(\omega', \mathbf{X}\left(T_j + \frac{t + 2\mathcal{T}(\mathbf{X}(T_j), \mathbf{z}^S)}{1 - \beta(T_j, \mathbf{z}^S)}\right), \mathbf{x}_s\right) \\ &\quad \times \exp\left(i\omega\left(T_j + \frac{t}{1 + \beta(T_j, \mathbf{z}^S)}\right) - i\omega'\left(T_j + \frac{t + 2\mathcal{T}(\mathbf{X}(T_j), \mathbf{z}^S)}{1 - \beta(T_j, \mathbf{z}^S)}\right)\right) d\omega d\omega' dt. \end{aligned}$$

Since  $\Delta T$  is larger than the coherence time of the noise sources, that is,  $B\Delta T \gg 1$ , the autocorrelation function is self-averaging and with the form of its autocorrelation function in the Fourier domain (29) we obtain:

$$\begin{aligned} \mathcal{I}_{\text{dpsa},j}(\mathbf{z}^S) &= \frac{1}{2\pi \Delta T} \int_{-\infty}^{\infty} \Pi\left(\frac{t}{\Delta T}\right) \int_{-\infty}^{\infty} \hat{F}(\omega) \overline{\hat{G}_0}\left(\omega, \mathbf{X}\left(T_j + \frac{t}{1 + \beta(T_j, \mathbf{z}^S)}\right), \mathbf{x}_s\right) \\ &\quad \times \hat{G}_0\left(\omega, \mathbf{X}\left(T_j + \frac{t + 2\mathcal{T}(\mathbf{X}(T_j), \mathbf{z}^S)}{1 - \beta(T_j, \mathbf{z}^S)}\right), \mathbf{x}_s\right) \\ &\quad \times \exp\left(-i\omega \frac{2\beta(T_j, \mathbf{z}^S)t}{1 - \beta^2(T_j, \mathbf{z}^S)} - i\omega \frac{2\mathcal{T}(\mathbf{X}(T_j), \mathbf{z}^S)}{1 - \beta(T_j, \mathbf{z}^S)}\right) d\omega dt. \end{aligned}$$

Using the high-frequency asymptotic form of the homogeneous Green's function (20), we get

$$\begin{aligned} \mathcal{I}_{\text{dpsa},j}(\mathbf{z}^S) &= \frac{c_0}{16\pi^2 \omega_0 \Delta T |\mathbf{X}(T_j) - \mathbf{x}_s|} \int_{-\infty}^{\infty} \int_{-\infty}^{\infty} \Pi\left(\frac{t}{\Delta T}\right) \hat{F}(\omega) \\ &\quad \times \exp\left(-i\omega \frac{|\mathbf{X}(T_j + \frac{t}{1 + \beta(T_j, \mathbf{z}^S)}) - \mathbf{x}_s|}{c_0} + i\omega \frac{|\mathbf{X}(T_j + \frac{t + 2\mathcal{T}(\mathbf{X}(T_j), \mathbf{z}^S)}{1 - \beta(T_j, \mathbf{z}^S)}) - \mathbf{x}_s|}{c_0}\right) \\ &\quad \times \exp\left(-i\omega \frac{2\beta(T_j, \mathbf{z}^S)t}{1 - \beta^2(T_j, \mathbf{z}^S)} - i\omega \frac{2\mathcal{T}(\mathbf{X}(T_j), \mathbf{z}^S)}{1 - \beta(T_j, \mathbf{z}^S)}\right) d\omega dt. \end{aligned}$$

We can expand the phase term as

$$\begin{aligned} &\frac{|\mathbf{X}(T_j + \frac{t}{1 + \beta(T_j, \mathbf{z}^S)}) - \mathbf{x}_s|}{c_0} - \frac{|\mathbf{X}(T_j + \frac{t + 2\mathcal{T}(\mathbf{X}(T_j), \mathbf{z}^S)}{1 - \beta(T_j, \mathbf{z}^S)}) - \mathbf{x}_s|}{c_0} \\ &= \beta(T_j, \mathbf{x}_s) \frac{2\mathcal{T}(\mathbf{X}(T_j), \mathbf{z}^S)}{1 - \beta(T_j, \mathbf{z}^S)} + O\left(\beta^2\left(\frac{L}{c_0} \vee t\right)\right), \end{aligned}$$

and therefore, after integrating in  $\omega$ :

$$\mathcal{I}_{\text{dpsa},j}(\mathbf{z}^S) = \frac{c_0}{8\pi\omega_0\Delta T|\mathbf{X}(T_j) - \mathbf{x}_s|} \int_{-\infty}^{\infty} \Pi\left(\frac{t}{\Delta T}\right) \times F\left(\frac{2\beta(T_j, \mathbf{z}^S)t}{1 - \beta^2(T_j, \mathbf{z}^S)} + \frac{2\mathcal{T}(\mathbf{X}(T_j), \mathbf{z}^S)(1 + \beta(T_j, \mathbf{x}_s))}{1 - \beta(T_j, \mathbf{z}^S)}\right) dt.$$

This integral is zero if the argument of  $F$  is always much larger than  $1/B$ , which happens if  $L/c_0 \gg \beta\Delta T + 1/B$ , which is equivalent to  $L \gg V\Delta T$  and  $BL/c_0 \gg 1$ , which holds true.

## References

- [1] M. ABRAMOWITZ AND I. STEGUN, *Handbook of mathematical functions*, Dover Publications, New York, 1965. 8, 18
- [2] M. ANTONIOU, M. CHERNIAKOV, AND C. HU, *Space-surface bistatic sar image formation algorithms*, IEEE Transactions on Geoscience and Remote Sensing, 47 (2009), pp. 1827-1843. 2
- [3] A. BAKULIN AND R. CALVERT, *The virtual source method: Theory and case study*, Geophysics, 71 (2006), pp. SI139-SI150. 2
- [4] L. BORCEA, M. MOSCOSO, G. PAPANICOLAOU, AND C. TSOGKA, *Synthetic aperture imaging of direction and frequency dependent reflectivities*, SIAM J. Imaging Sciences, 9 (2016), pp. 52-81. 22
- [5] A. CAPOZZOLI, C. CURCIO, AND A. LISENO, *Fast GPU-based interpolation for SAR backprojection*, Progr. Electromagn. Res., 133 (2013), pp. 259-283. 2
- [6] C. H. CASTEEL JR, L. R. A. GORHAM, M. J. MINARDI, S. M. SCARBOROUGH, K. D. NAIDU, AND U. K. MAJUMDER, *A challenge problem for 2d/3d imaging of targets from a volumetric data set in an urban environment*, in Proceedings of SPIE, volume 6568, page 65680D, 2007. 4
- [7] M. CHENEY, *A mathematical tutorial on synthetic aperture radar*, SIAM Review, 43 (2001), pp. 301-312. 17
- [8] J. C. CURLANDER AND R. N. McDONOUGH, *Synthetic aperture radar*, Wiley, New York, 1991. 17
- [9] A. FARINA AND H. KUSCHEL, *Guest editorial special issue on passive radar (Part I)*, IEEE Aerospace and Electronic Systems Magazine, 27 (2012), issue 10. 2, 4
- [10] J. GARNIER AND G. PAPANICOLAOU, *Passive sensor imaging using cross correlations of noisy signals in a scattering medium*, SIAM J. Imaging Sciences, 2 (2009), pp. 396-437. 2, 5, 6
- [11] J. GARNIER AND G. PAPANICOLAOU, *Correlation based virtual source imaging in strongly scattering media*, Inverse Problems, 28 (2012), 075002. 2
- [12] J. GARNIER AND G. PAPANICOLAOU, *Role of scattering in virtual source array imaging*, SIAM J. Imaging Sciences, 7 (2014), pp. 1210-1236. 2
- [13] J. GARNIER AND G. PAPANICOLAOU, *Passive synthetic aperture imaging*, SIAM J. Imaging Sci., 8 (2015), pp. 2683-2705. 2, 3, 4, 5, 14, 15
- [14] J. GARNIER AND G. PAPANICOLAOU, *Passive imaging with ambient noise*, Cambridge University Press, Cambridge, 2016. 2
- [15] H. GUO, K. WOODBRIDGE, AND C. J. BAKER, *Evaluation of WiFi beacon transmissions for wireless based passive radar*, in: Proc. of 2008 IEEE Radar Conference, 2008. 2
- [16] J. HOMER, K. KUBIK, B. MOJARRABI, I. LONGSTAFF, E. DONSKOI, AND M. CHERNIAKOV, *Passive bistatic radar sensing with leos based transmitters*, in: Proceedings of IEEE International Geoscience and Remote Sensing Symposium, vol. 1, 2002, pp. 438-440. 2
- [17] G. LI, J. XU, Y. N. PENG, AND X. G. XIA, *Bistatic linear array SAR for moving target detection, location and imaging with two passive airborne radars*, IEEE Transactions on Geoscience and Remote Sensing, 45 (2007), pp. 554-565. 2

- [18] N. C. MAKRIS, F. INGENITO, AND W. A. KUPERMAN, *Detection of a submerged object insonified by surface noise in an ocean waveguide*, J. Acoust. Soc. Am., 96 (1994), pp. 1703-1724. [2](#)
- [19] P. ROUX, W. A. KUPERMAN, AND THE NPAL GROUP, *Extracting coherent wave fronts from acoustic ambient noise in the ocean*, J. Acoust. Soc. Am., 116 (2004), pp. 1995-2003. [2](#)
- [20] G. T. SCHUSTER, *Seismic interferometry*, Cambridge University Press, Cambridge, 2009. [2](#)
- [21] M. SIDERIUS, C. H. HARRISON, AND M. B. PORTER, *A passive fathometer technique for imaging seabed layering using ambient noise*, J. Acoust. Soc. Am., 120 (2006), pp. 1315-1323. [2](#)
- [22] S. V. TSYNKOV, *On the use of Start-Stop approximation for spaceborne SAR imaging*, SIAM J. Imaging Sciences, 2 (2009), pp. 646-669. [2](#)
- [23] L. WANG, C. E. YARMAN, AND B. YAZICI, *Doppler-Hitchhiker: A novel passive synthetic aperture radar using ultranarrowband sources of opportunity*, IEEE Transactions on Geoscience and Remote Sensing, 49 (2011), pp. 3521-3537. [2](#), [3](#), [6](#)
- [24] L. WANG, C. E. YARMAN, AND B. YAZICI, *Theory of passive synthetic aperture imaging*, in Excursions in Harmonic Analysis, Volume 1, Applied and Numerical Harmonic Analysis, 2013, pp. 211-236. [2](#), [3](#), [6](#), [22](#)
- [25] K. WAPENAAR, E. SLOB, R. SNIEDER, AND A. CURTIS, *Tutorial on seismic interferometry: Part 2 - Underlying theory and new advances*, Geophysics, 75 (2010), pp. A211-A227. [2](#)
- [26] C. YARMAN, L. WANG, AND B. YAZICI, *Doppler synthetic aperture hitchhiker imaging*, Inverse Problems, 26 (2010), 065006. [2](#), [3](#), [6](#)
- [27] C. YARMAN AND B. YAZICI, *Synthetic aperture hitchhiker imaging*, IEEE Transactions on Imaging Processing, 17 (2008), pp. 2156-2173. [2](#), [3](#), [6](#)